Electrochemistry Communications 177 (2025) 107985

Contents lists available at ScienceDirect

Electrochemistry Communications

journal homepage: www.elsevier.com/locate/elecom

Short Communication

One-step atmospheric microplasma synthesis of an NMC-type lithium-ion battery cathode

Ryan Brow *, Chaiwat Engtrakul, Kae Fink, Nicholas McKalip, Maxwell Schulze, Andrew Colclasure

Center for Energy Conversion and Storage Systems, National Renewable Energy Laboratory, Golden, CO 80401, United States

ARTICLE INFO

Keywords:
Plasma synthesis
Atmospheric microplasma
One-step synthesis
Lithium-ion cathode
NMC

ABSTRACT

The manufacture of battery cathode materials is the most energy-intensive step in the production of commercial lithium-ion batteries; specifically, the synthesis of the widely used transition metal oxide cathodes can require tens of hours at temperatures exceeding 700 °C. Attempts to limit the reaction time and energy required to form crystalline cathode materials often still include a heating or calcination step. This communication aims to highlight a nascent yet novel synthesis route: a one-step atmospheric microplasma process for synthesizing cathode particles in less than one second. The hollow-tube reactor employed produces crystalline particles measuring 0.1–3 μm in diameter, displays narrow XRD peaks corresponding to the 003, 104, and 101 planes, and exhibits anodic redox behavior at 3.75 V vs. lithium—characteristic of transition-metal oxide cathode materials—all without requiring an additional calcination step.

1. Introduction

Conventional synthesis of lithium-ion battery cathodes at the industrial scale involves mixing precursors, followed by extensive heat treatment that accounts for nearly 90 % of the energy consumption in cell manufacturing [1]. A typical synthesis routine for the manufacture of ternary metal oxide (e.g., NMC) cathodes uses co-precipitation, in which a liquid solution of metal hydroxides or metal sulfates is continuously stirred above 50 °C and pH >10 in a controlled atmosphere. The metal hydroxide precipitate is collected, mixed with a lithium source, and calcined at temperatures >700 °C. It is estimated that this heating step accounts for 47 % of the final cost of the cell [1].

Plasma synthesis offers a possible way to decrease the cost, energy, and emissions required to synthesize these transition metal oxide cathode materials. Plasma synthesis involves the use of localized, high-energy plasma discharges to induce chemical reactions and manipulate the growth of materials. Plasma synthesis is currently used to synthesize a wide range of metal nanoparticles (including nickel, silicon, gold, iron, and platinum [2–6]) and metal oxide nanoparticles (including nickel oxide, zinc oxide, and silicon dioxide [7–9]) using a variety of techniques: plasma-enhanced chemical vapor deposition, dielectric barrier discharge, plasma jet, and in/on-solution plasma [10–13].

Plasma-type synthesis has also been used to form a variety of cathode materials. For example, plasma-based processes have been utilized to apply nanosized carbon coatings on lithium iron phosphate (LFP) cathodes, which can increase electronic conductivity from 5×10^{-7} to 1×10^{-2} S/cm [14]. Lithium metal oxide nanoparticles, including $LiMn_2O_4$ with a truncated octahedral morphology, were synthesized using an induction thermal plasma by co-introducing Li_2CO_3 and preformed metal oxide solids into the plasma [15]. Perhaps most impressively, NMC 262 cathodes were synthesized via atmospheric spray pyrolysis and maintained a discharge capacity of 210 mAh/g after 50 cycles. In this case, metal nitrates were introduced into a microwave plasma to form NMC powders. Unfortunately, the powders still required a 5-h bake at 900 °C for lithiation [16].

Presented here is a truly one-step atmospheric microplasma process used to synthesize NMC-type cathode particles. A hollow-tube reactor design produces spherical NMC-type particles that vary in diameter from 0.1 to 3 μm. The particles have a relatively featureless spherical morphology as shown in SEM and have XRD patterns consistent with the layered structure of NMC-type cathodes. Particles also exhibit expected redox activity when placed versus Li^0 – without requiring additional heating or calcination—a key distinction from previous plasma-based methods that typically still demand high-temperature processing. Despite the inconsistent plasma discharge observed during this synthesis

* Corresponding author.
E-mail address: Ryan.Brow@NREL.gov (R. Brow).

https://doi.org/10.1016/j.elecom.2025.107985
Received 16 December 2024; Received in revised form 17 June 2025; Accepted 21 June 2025
Available online 23 June 2025
1388-2481/© 2025 The Authors. Published by Elsevier B.V. This is an open access article under the CC BY license (http://creativecommons.org/licenses/by/4.0/).

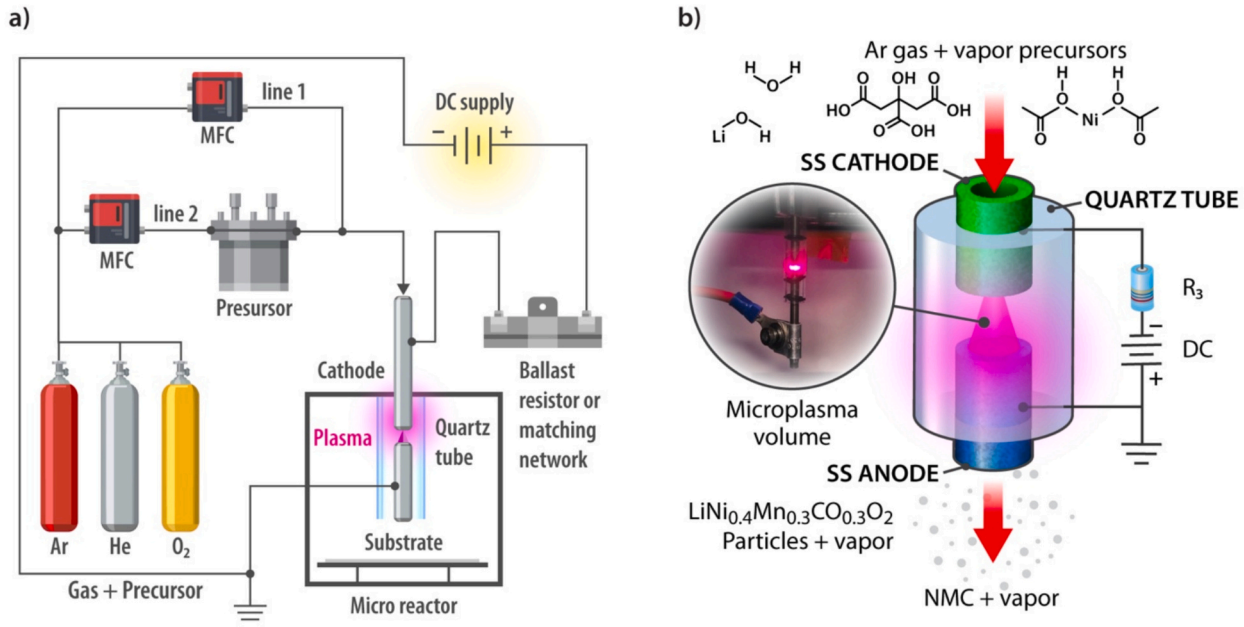

Fig. 1. Schematic of the hollow-tube reactor (a). A cartoon and image of the reaction vessel (b).

method, substantial evidence indicates that NMC-type cathode materials were successfully synthesized. This communication is intended as a demonstration of a novel and promising approach for energy-efficient cathode synthesis using atmospheric microplasma, highlighting a truly one-step synthesis route in development.

2. Material synthesis and cell fabrication

A hollow-tube reactor (Fig. 1) was used to synthesize NMC cathode particles via a one-step atmospheric microplasma route. Argon and oxygen gases were used as both the plasma gas and the carrier gas for the precursor vapor. The sol of a sol-gel-type NMC synthesis was used as the liquid precursor, previously reported [17]. The sol contained a 0.3 M mixture of nickel, cobalt, and manganese acetate hydrates with a stoichiometry of $Ni_{0.5}Co_{0.3}Mn_{0.2}$ (Sigma Aldrich). Citric acid was used as a chelating agent, and lithium hydroxide hydrate (Sigma Aldrich) was used as the lithium source yielding a total solution composition of $Li_{1.1}Ni_{0.5}Mn_{0.3}Co_{0.2}$ in DI water. The liquid precursor solution was vaporized at RT using a sonicator into a vapor chamber, where it was then carried by argon gas into the reactor vessel. A 250 W, 25 kHz power supply was used to provide 3 kV between the cathode and anode electrodes (Fig. 1a) that were spaced approximately 1.0–1.5 mm apart. A ballast resistor (500 kΩ) and potentiometer (0–100 kΩ) were utilized to limit current and maintain glow discharge. The stainless-steel cathode (1 mm I.D.) and anode (1.5 mm I.D.) tubes were held in a quartz tube with a variable 0–3 mm spacing between them. Samples were collected at the base of the anode electrode. With the potentiometer at 0 kΩ and an Ar-only flow of 30 sccm, an arc-like plasma ignites; by gradually increasing the potentiometer's resistance, it transitions into a stable glow discharge. The precursor vapor was then slowly introduced and held at the final rate (10–100 sccm).

Battery electrodes were fabricated by mixing carbon black with PVDF in NMP (Sigma Aldrich) and depositing the slurry onto Al foil using a doctor blade. The electrodes were dried in vacuum overnight and assembled versus lithium metal and Gen-2 electrolyte (1.2 M $LiPF_6$ in 3:7 wt:wt ethylene carbonate:ethylmethyl carbonate). The separator used was Celgard 2500. Material was collected by placing a container of amorphous carbon (MTI Corp.) under the microplasma reactor and collecting reaction products. The mass of the reaction products was determined by taking the difference in mass before and after collection.

3. Results and discussion

3.1. SEM

Scanning electron microscopy was used to visualize the synthesis products. Evenly distributed, spherical particles can be seen with particle diameters varying between 0.1 and 3 μm (Fig. 2). The large size of at least some of the particles suggests an advantage for the method of atmospheric microplasma: namely, atmospheric microplasma yields particle sizes much larger than those typically produced using low/mid-range vacuum plasmas, typically in the nm range [18]. Microplasma-synthesized particles have smooth, featureless surfaces, unlike traditional calcination products, which form large agglomerates of loosely bound primary particles [19]. Additionally, the spherical particles produced by microplasma synthesis are devoid of any obvious (0 0 1), (0 1 2), or (1 0 4) facets that would be expected of a single crystalline particle, suggesting the particles are polycrystalline. The smooth texture of the particles suggests that the particles reported here are made of smaller crystallites that are more tightly bound, fused, or have been etched. This unique morphology may have important implications for rate capability and durability.

Basic elemental analysis was performed via energy-dispersive X-ray spectroscopy (Fig. 2e). Conductive carbon tape was placed under the reactor and allowed to collect material for 5 min. Two regions were examined: Region A and Region B (Fig. 2d). Region A contained a spherical particle similar to that shown in Fig. 2a–b. Region B contained no particle. Region A contains the expected elements of interest: nickel, manganese, and cobalt in the approximate stoichiometry ($Ni_4Mn_3Co_3$) of that found in the precursor solution ($Ni_5Mn_3Co_2$). Region B contained

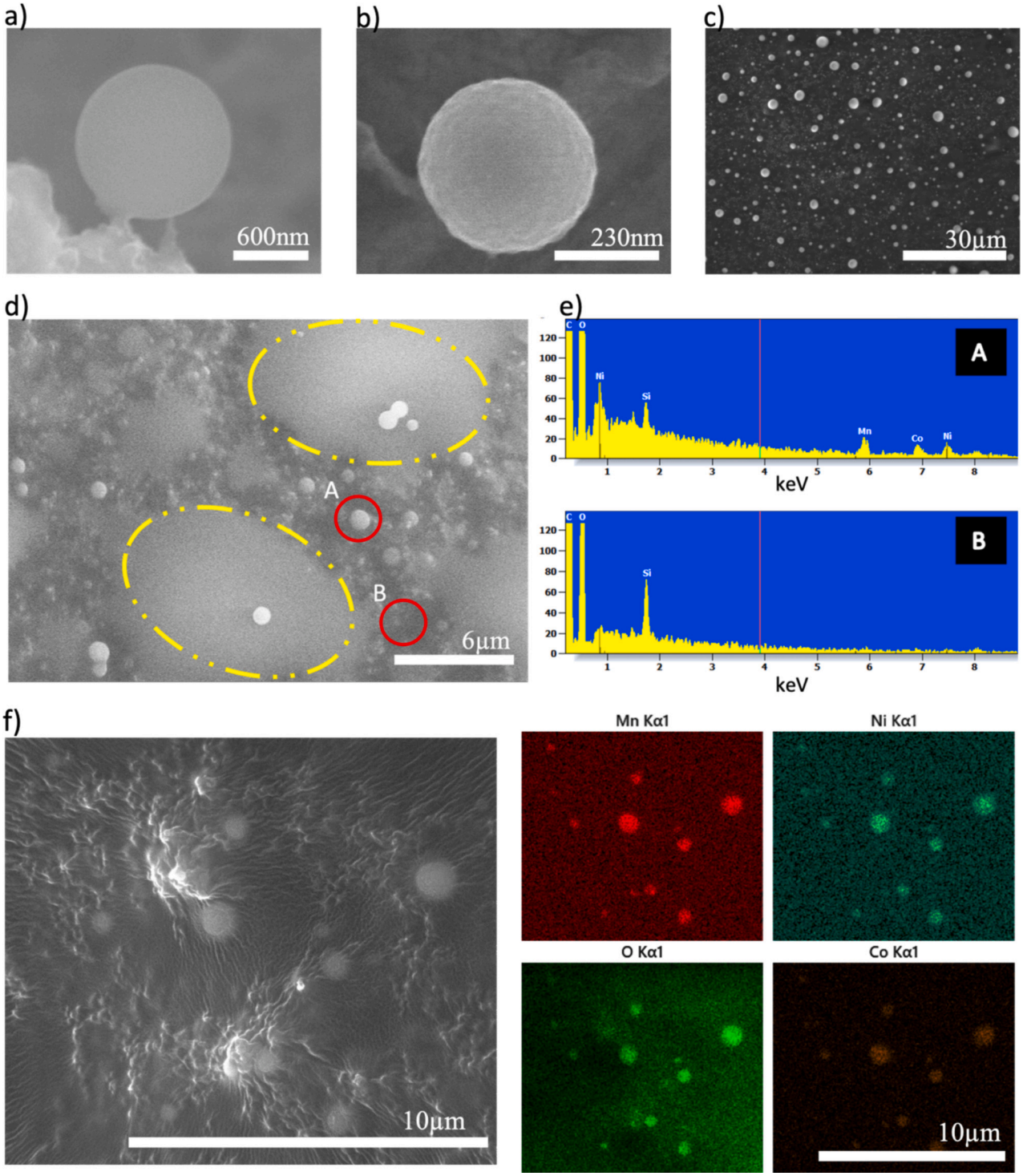

Fig. 2. Scanning electron microscopy (SEM) images show size (a), surface morphology (b), and distribution (c) of microplasma reaction products. Unreacted precursor vapor can be seen in the dashed yellow circle (d) and EDX spectra of a region containing a particle (image "d" region A) and no particle (image "d" region B) can be seen in (e). EDX map of several NMC-type particles and their elemental makeup (f). (For interpretation of the references to color in this figure legend, the reader is referred to the web version of this article.)

no discernible amount of any transition metal. Interestingly, this sample contained what appeared to be unreacted precursor that had dried into amorphous clumps on the substrate (yellow circles).

3.2. XRD

A silicon zero-background plate was placed under the reactor vessel for 15 min and allowed to collect reaction products. The deposit had a milky-like color with no visible particles. The samples were placed into a Rigaku SmartLab system with a Cu-kα source (Fig. 3). While the degree of crystallinity of NMC-type cathodes – generally determined from the splitting of the (0 1 8)/(1 1 0) and (0 0 6)/(0 1 2) peaks – is difficult to determine due to the low signal-to-noise ratio of the diffractogram (caused by the limited amount of material present), the presence of

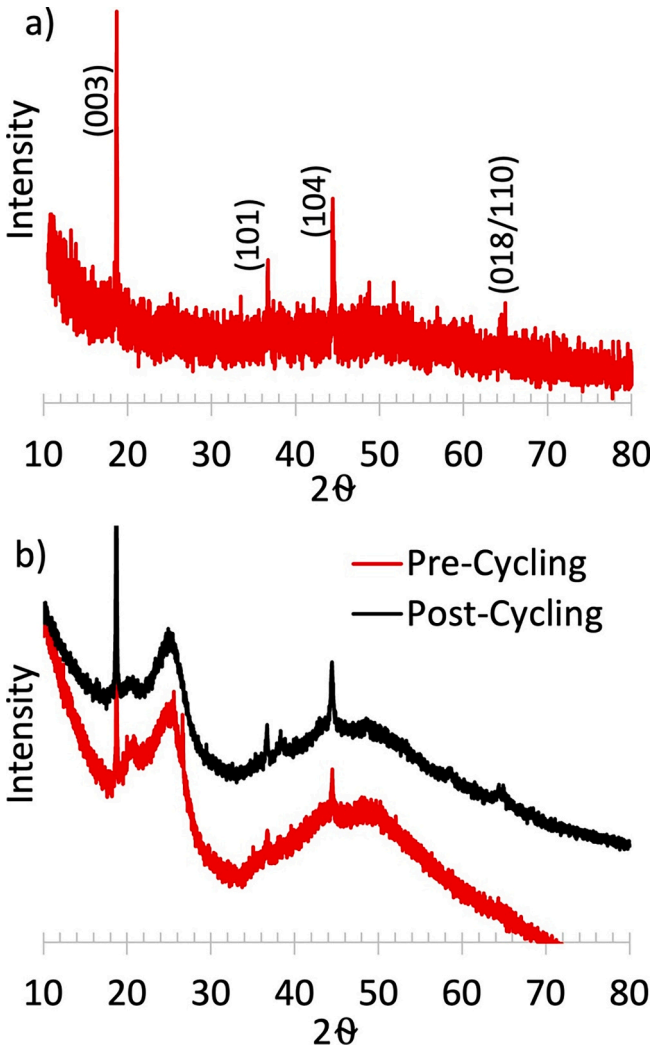

Fig. 3. X-ray diffraction data from Cu-kα source with reaction products collected on a silicon zero-background substrate. Diffractogram suggests reaction products are at least partially crystalline NMC-type cathode.

peaks at 18.7, 44.5, and 64.9 2θ (the (0 0 3), (1 0 4), and (0 1 8/1 1 0) peaks respectively) suggests that the material is at least partially crystalline and has the expected hexagonal lattice structure with the $R\bar{3}m$ space group [20]. The particles also appear to be phase-pure, as there are no peaks associated with metallic or metal-oxide nanoparticles or recrystallized lithium hydroxide [7,21]. The broad peak centered at 50 2θ can be attributed to the silicon zero-background substrate, and the signal contains a large X-ray fluorescence from nickel. Unfortunately, the low signal-to-noise ratio (3:1) prevents accurate Rietveld refinement.

3.3. Electrochemical testing

Cyclic voltammetry was used to determine the redox behavior of the cathode particles synthesized via atmospheric microplasma. Small amounts of carbon black were placed under the reactor for 15 min, mixing the carbon black every two minutes. Two different samples were prepared: one with the vapor precursor flowing *with* plasma lit, and a control with the vapor precursor flowing but *without* plasma. Each sample of carbon black was then slurry-coated by mixing with PVDF in NMP and depositing onto Al foil using a doctor blade to make a cathode electrode. The electrodes were dried in vacuum overnight and assembled versus lithium metal and Gen-2 electrolyte (1.2 M $LiPF_6$ in 3:7 wt: wt ethylene carbonate:ethylmethyl carbonate).

For the sample flowing through plasma, parameters included an argon flow of 25 sccm, voltage of 3000 V, 1.5 mm electrode gap, and 500 kΩ ballast resistor. It was difficult to maintain a glow discharge, and the plasma displayed a glow-to-arc discharge, as described previously [22], for most of the experiment. This may have caused large amounts of electrode sputtering as evidenced by the iron redox peak clearly visible in Fig. 4a. $Iron^{2+/3+}$ has an anodic redox potential of 3.6 V and cathodic potential at 3.28 V at finite diffusion or slow scan rates vs lithium [23]. This peak masks that of Ni, so a slower anodic CV scan was performed and scanned near the expected Ni potential (Fig. 4b). Here, redox from both the control cell (where the precursor vapor had not been exposed to plasma) and the cell with plasma-processed products can both be seen. There is a clear anodic peak at the expected potential of Ni redox for this slow scan speed, suggesting that some quasi-reversible nickel-based redox was still occurring in the iron-rich sample [24].

To avoid the glow-to-arc type discharge and electrode sputtering

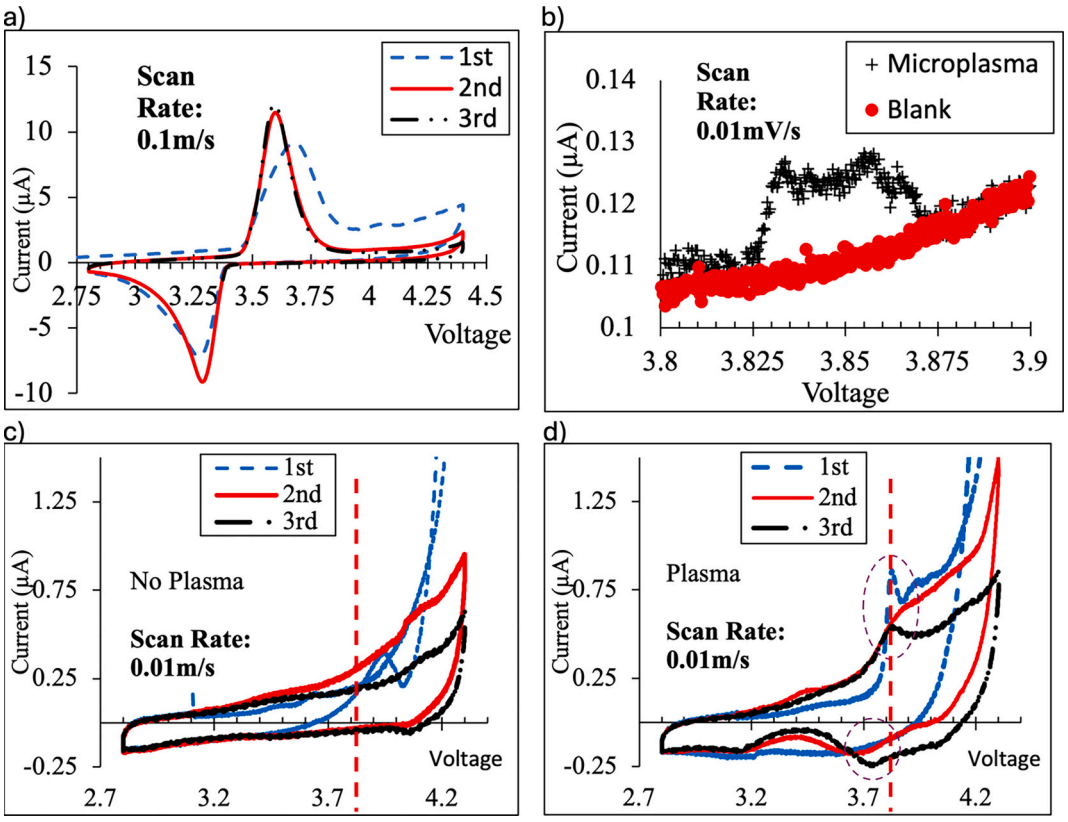

Fig. 4. Cyclic voltammetry (CV) of reaction products collected during arc-like plasma discharge showing iron redox behavior (a). Slow CV scans of sample represented in "a" showing nickel redox (b). Slow CV scans of reaction products collected *without* plasma (c) and after adding additional resistance to obtain a more glow-like plasma discharge (d).

mentioned above, additional variable resistance (0–100 kΩ) was added in series with the ballast resistor. In this configuration, the plasma was struck with the variable resistor set to 0 kΩ and then the resistance was increased (typically ~50 kΩ) until a plasma with a more glow-like discharge became clearly visible. Again, two samples of carbon black – one taken while the vapor precursor was flowing through the system but *no* plasma lit, and the other with vapor precursor flowing and the plasma *lit* – were placed underneath the reactor for 15 min and made into cells as stated above. The cyclic voltammetry of the two cells can be seen in Fig. 4c–d. Here, the quasi-reversible Ni anodic/cathodic redox peaks are observed at 3.85 V and 3.7 V, respectively (purple dashed circle). Their electrochemical quasi-reversibility, combined with the XRD peaks shown in Fig. 3, indicates that NMC-type cathode particles have been successfully formed and can be effectively cycled in a half-cell.

To further evaluate the electrochemical behavior of these NMC-type particles, coin cells were fabricated and cycled (2.8–4.4 V) at C/10 charge and discharge rates in Gen-2 electrolyte versus lithium metal. Discharge capacities of approximately 125 mAh/g were obtained for these cells (Fig. 5a). The lower-than-expected discharge capacity is most likely due to a combination of low crystal quality and unreacted precursor (mentioned above) that does not contribute to reversible electrochemical behavior. This can be more clearly seen in differential capacity plots (DQ/DV) for cells that contain precursor that *was not* exposed to plasma (Fig. 5b) and precursor that *was* exposed plasma (Fig. 5c). Here, the effect of the plasma synthesis can be seen most clearly. Cells that contain precursor vapor that was not exposed plasma treatment have no obvious redox peaks other than those of electrolyte decomposition. However, the precursor exposed to glow discharge has clear redox peaks characteristic of an NMC-type cathode material, specifically the wide oxidation peak of $Ni^{2+}/Ni^{3+}/Ni^{4+}$ and Co^{3+}/Co^{4+} at 3.70 and 3.75 V, respectively [25].

4. Conclusion

To our knowledge – for the first time – a *one-step* synthesis of an NMC-type cathode has been accomplished via atmospheric microplasma. A hollow-tube reactor was used to create NMC cathode particles that display crystallinity and the expected redox behavior. The secondary structure of the produced particles appears to consist of more tightly bound primary particles, which may help mitigate particle cracking; however, further testing is required to confirm this. Although the reactor setup used in this study successfully created cathode particles, the quantities were exceedingly small. Additionally, inconsistent plasma conditioning made it difficult to produce material reliably. Future work should focus on maintaining plasmas with more consistent glow-like discharges, gaining insight into the synthesis mechanism, investigating electrodeless designs, and building microplasma arrays for scale-up.

CRediT authorship contribution statement

Ryan Brow: Writing – original draft, Methodology, Investigation, Formal analysis, Data curation, Conceptualization. **Chaiwat Engtrakul:**

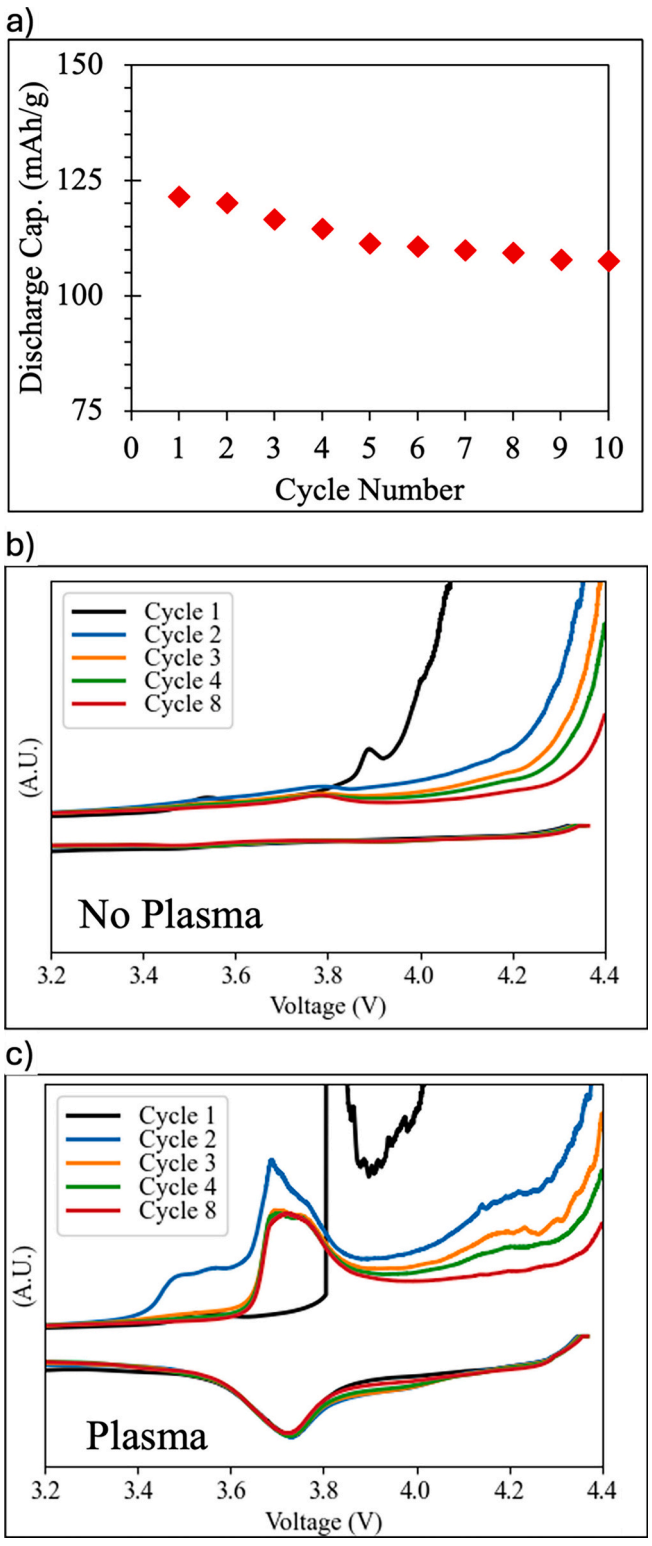

Fig. 5. The discharge capacity of NMC-type particles deposited onto amorphous carbon and then assembled into coin cells vs Li metal (a). DQ/DV of coin cells containing reaction products collected *without* (b) and *with* (c) glow-type plasma discharge. The y-axis (arbitrary units) of the DQ/DV plots is to the same scale.

Conceptualization, Methodology. **Kae Fink:** Writing – review & editing, Formal analysis. **Nicholas McKalip:** Writing – review & editing, Formal analysis, Data curation. **Maxwell Schulze:** Writing – review & editing, Formal analysis, Data curation. **Andrew Colclasure:** Writing – review & editing, Supervision, Project administration, Formal analysis.

Declaration of competing interest

The authors declare the following financial interests/personal relationships which may be considered as potential competing interests: Ryan Brow has patent pending. If there are other authors, they declare that they have no known competing financial interests or personal relationships that could have appeared to influence the work reported in this paper.

Acknowledgments

This work was authored by the Alliance for Sustainable Energy, LLC, the manager and operator of the National Renewable Energy Laboratory for the US Department of Energy (DOE) under contract No. DE-AC36-08GO28308 and funded by the Laboratory Directed Research and Development program. The views expressed in the article do not necessarily represent the views of the DOE or the US government. The US government and the publisher, by accepting the article for publication, acknowledge that the US government retains a nonexclusive, paid-up, irrevocable, worldwide license to publish or reproduce the published form of this work, or allow others to do so, for US government purposes.

Data availability

Data will be made available on request.

References

[1] H.E. Melin, Analysis of the climate impact of lithium-ion batteries and how to measure it, 2019.
[2] A. Woodard, et al., Plasma Processes Polym. 15 (2018) 1700104, https://doi.org/10.1002/ppap.201700104.
[3] L.M. Wheeler, et al., Chem. Mater. 27 (2015) 6869–6878, https://doi.org/10.1021/acs.chemmater.5b03309.
[4] D. Sun, et al., Langmuir 35 (2019) 4577–4588, https://doi.org/10.1021/acs.langmuir.8b03945.
[5] S.L. Girshick, et al., J. Aerosol Sci. 24 (1993) 367–382, https://doi.org/10.1016/0021-8502(93)90009-X.
[6] M. Cui, et al., Chem. Eng. J. 460 (2023) 141676, https://doi.org/10.1016/j.cej.2023.141676.
[7] S. Chakrabarti, et al., Nanoscale Adv. 1 (2019) 4915–4925, https://doi.org/10.1039/C9NA00299E.
[8] G. Primc, K. Brenčič, M. Mozetič, M. Gorjanc, Nanomaterials (Basel) 11 (2021), https://doi.org/10.3390/nano11051191.
[9] G. Kholodnaya, D. Ponomarev, R. Sazonov, G. Remnev, Radiat. Phys. Chem. 103 (2014) 114–118, https://doi.org/10.1016/j.radphyschem.2014.05.048.
[10] H. Yasaman, M. Prathyushakrishna, J.B. Timothy, R.N. Rajesh, C.V. Milana, *Chemical Vapor Deposition* (ed Neralla Sudheer), Ch. 10, IntechOpen, 2016.
[11] J. Li, et al., Nanomaterials (Basel) 9 (2019), https://doi.org/10.3390/nano9101428.
[12] A. Schutze, et al., IEEE Trans. Plasma Sci. 26 (1998) 1685–1694, https://doi.org/10.1109/27.747887.
[13] N. Saito, M.A. Bratescu, K. Hashimi, Jpn. J. Appl. Phys. 57 (2018) 0102A0104, https://doi.org/10.7567/JJAP.57.0102A4.
[14] I. Stenina, P. Minakova, T. Kulova, A. Yaroslavtsev, Batteries 8 (2022) 111.
[15] M. Tanaka, et al., Nanomaterials 6 (2016).
[16] B.P. Ajayi, A.K. Thapa, U. Cvelbar, J.B. Jasinski, M.K. Sunkara, Chem. Eng. Sci. 174 (2017) 302–310, https://doi.org/10.1016/j.ces.2017.09.022.
[17] C. Xiong, F. Liu, J. Gao, X. Jiang, ACS Omega 5 (2020) 30356–30362, https://doi.org/10.1021/acsomega.0c02807.
[18] J. Joseph, et al., Adv. Mater. Technol. 3 (2018) 1800070, https://doi.org/10.1002/admt.201800070.
[19] J. Zheng, P. Yan, L. Estevez, C. Wang, J.-G. Zhang, Nano Energy 49 (2018) 538–548, https://doi.org/10.1016/j.nanoen.2018.04.077.

[20] R. Weber, C.R. Fell, J.R. Dahn, S. Hy, J. Electrochem. Soc. 164 (2017) A2992, https://doi.org/10.1149/2.0441713jes.
[21] M. Takeuchi, R. Kurosawa, J. Ryu, M. Matsuoka, ACS Omega 6 (2021) 33075–33084, https://doi.org/10.1021/acsomega.1c05379.
[22] A.I. Saifutdinov, Plasma Sources Sci. Technol. 31 (2022) 094008, https://doi.org/10.1088/1361-6595/ac89a7.
[23] C. Gao, J. Zhou, G. Liu, L. Wang, J. Mater. Sci. 52 (2017) 1590–1602, https://doi.org/10.1007/s10853-016-0453-z.
[24] X. Li, et al., Energ. Environ. Sci. 7 (2014) 768–778, https://doi.org/10.1039/C3EE42704H.
[25] M. Dixit, et al., Phys. Chem. Chem. Phys. 18 (2016) 6799–6812, https://doi.org/10.1039/C5CP07128C.